Boarding Control System - for Improved Accessibility to Offshore Wind Turbines

Øyvind F. Auestad [*,***] **Tristan Perez** [**] **Jan T. Gravdahl** [*]
Asgeir J. Sørensen [****] **Trygve H. Espeland** [***]

[*] *Dept. of Eng. Cybernetics, O. S. Bragstads plass D, NTNU, N-7491 Trondheim, Norway; e-mail: oyvind.auestad@itk.ntnu.no*
[**] *Robotics, Science and Engineering Faculty, QUT, Brisb., Australia*
[***] *Umoe Mandal AS Gismerøyveien 205, N-4515 Mandal, Norway*
[****] *Centre for Autonomous Marine Operations (AMOS), Dept. of Marine Technology, Otto Nielsens vei 10, NTNU, N-7491, Trondheim, Norway*

Abstract: This paper considers the dynamic modelling and motion control of a Surface Effect Ship (SES) for safer transfer of personnel and equipment from vessel to-and-from an offshore wind-turbine. Such a vessel is a key enabling factor for operation and maintenance (O&M) of offshore wind-energy infrastructure. The control system designed is referred to as Boarding Control System (BCS). We investigate the performance of this system for a specific wind-farm service vessel—The Wave Craft. A two-modality vessel model is presented to account for the vessel free motion and motion whilst in contact with a wind-turbine. On a SES, the pressurized air cushion carries the majority of the vessel mass. The control problem considered relates to the actuation of the pressure such that wave-induced vessel motions are minimized. This leads to a safer personnel transfer in developed sea-states than what is possible today. Results for the BCS is presented through simulation and model-scale craft testing.

Keywords: Modelling and identification, Offshore systems modelling and control, High speed vessels

1. MOTIVATION AND INTRODUCTION

As reported by the European Environment Agency's EEA (2008), it is expected that in 2020 there will be 30-40 times the installed offshore-wind infrastructure developed in 2008. The next generation of turbines are located significantly further offshore. Therefore, they experience higher sea states, which requires specialised service vessels for operation and maintenance (O&M). A key issue for good economics on an offshore wind farm is maximization of access feasibility for O&M. Surface Effect Ship (SES) equipped with the Boarding Control System (BCS) introduced in this paper will allow safer transfer of personnel and equipment from vessel to-and-from an offshore wind-turbine.

Based on our modelling and experimental validation (for data corresponding to the British North Sea), we estimate that a relatively small craft can enable safe turbine access in sea states of up to 2.5 meter significant wave height. Today, a similar sized craft can only operate safely up to 1.5 meters (OWA, 2010). This improvement in vessel motion handling would significantly extend the operability envelope.

1.1 Surface effect ships

The SES rides on an air cushion which is enclosed by two rigid catamaran demi-hulls and flexible rubber seals at the bow and the stern. SES literature can be found in Lavis (1998); Butler (1985); Kaplan et al. (1981). Fig. 1 shows a cutaway drawing along the longitudinal centre plane of a typical SES.

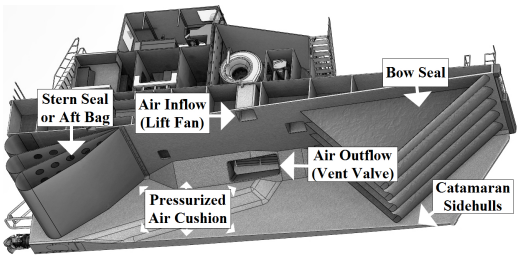

Fig. 1. Cutaway drawing along the longitudinal centre plane of a typical SES. Illustration: Umoe Mandal.

The air cushion is pressurized by centrifugal lift fans that blow air into the cushion. The air cushion lifts the vessel vertically and the pressurized cushion can carry up to 80% of the total vessel mass. When this is the case, only a minor part of the hull is submerged and exposed to hydrodynamic drag. In this case, the pressure is controlled by controlling the position of a set of vent valves that varies the cushion air leakage. This can alter the crafts submerged level considerably. To obtain high performance during turbine boarding, a Wave Craft has installed twice the air-flow actuation capacity necessary for traditional SES high-speed mode. This is the consequence of the BCS needing to transfer large amount of air through each wave in order to achieve crucial vertical motion damping. Fig.

2 shows a model-test boarding setup. For cushion control systems during transit, or *Ride Control Systems (RCS)*, see Adams et al. (1983); Sørensen and Egeland (1995); Kaplan and Davies (1978).

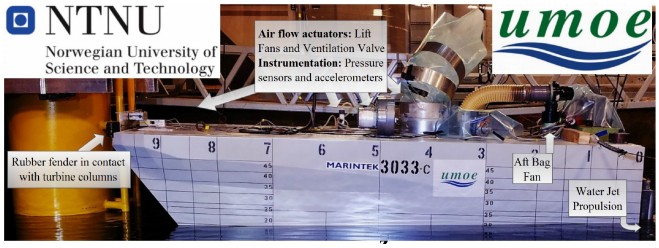

Fig. 2. The Wave Craft model test (photo: Umoe Mandal)

2. MATHEMATICAL MODELLING

In this section, we develop a mathematical model that accounts for both free station keeping and station keeping whilst the vessel bow is in contact with the wind-turbine column. The following are the modelling hypotheses considered:

(1) Vessel motion in surge, heave and pitch. The wind-turbine column is considered vertical and rigid.

(2) As a point of reference on the vessel, we consider the point B which is located below the center-of-gravity on the mean water line. The surge and heave displacements at point B are considered with respect to the point O in an inertial (i) frame, namely $x^i_{B/O}$ and $z^i_{B/O}$. The upper right script indicate the coordinate system and the lower scripts indicate the reference points to which these offsets refer to. This is illustrated in Fig. 3.

(3) The compliance of the point of contact between vessel and turbine is modelled by a vertical and a horizontal spring-damper system, k_v, c_v, k_h and c_h, respectively. The springs capture the elasticity of the bow rubber fender (Fig. 2 and 3). The springs are attached, or suspended, to a small fictitious mass m_*—which is considered in order to avoid computational causality issues due to holonomic constraints. The location of the uncompressed fictitious mass is represented by the point M, which is horizontally fixed, but but it has a vertical degree of freedom. Fig. 3 shows the system when there is no contact between vessel and turbine.

(4) The point C is located at the bow tip on the craft's centerline. The offsets $x^b_{C/B}$ and $z^b_{C/B}$ indicate the fixed distance between point C and B in body-fixed coordinates.

(5) We choose O to coincide with B when the horizontal spring is compressed. When turbine contact isn't present, we assume that our model, with the chosen coordinate frame, is valid given that the bow is arbitrarily close to the turbine. This is illustrated in Fig. 3. Hence, the model covers both in- and not in-turbine contact mode.

(6) The horizontal spring produces force (X^i_s) only when it is in compression which is when $x^i_{C/O} > x^i_{M/O}$, see Fig. 4. When this is the case, the vertical spring force Z^i_s, can act both in compression and tension. The spring suspension is fixed in the x-direction, hence $x^i_{M/O}$ is constant.

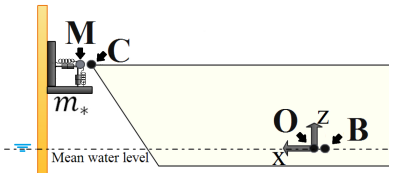

Fig. 3. Uncompressed horizonal spring - no contact

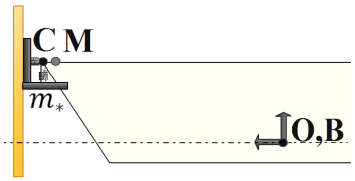

Fig. 4. Compressed horizontal spring - turbine contact

(7) During boarding operation, when contact is present, the bow $(z^i_{C/O})$ can either be fixed to, or slide up and down the wind-turbine column. This is regarded as stick-slip motion and is modelled as Coulomb friction force, which is calculated as the friction coefficient multiplied by the normal force between two bodies.

The stick motion relates to the static regime. When sufficient wave energy is available to overcome static friction, the bow will move either up or down and the system enters the kinetic regime. To account for this, we consider the following modes:

(a) Static friction, with coefficient μ_s, prevails if the mass m_* is fixed to the turbine, hence $\dot{z}^i_{M/O} = 0$.

(b) Kinetic friction, with coefficient μ_k prevails if m_* glides up and down the wind turbine column, hence $\dot{z}^i_{M/O} \neq 0$.

2.1 Spring forces

The pitch angle is referred to as $\theta(t)$ and is defined positive with the bow down according to the right-hand rule. The inertial coordinates for the point C can be expressed using a rotation matrix:

$$r^i_{C/O} = r^i_{B/O} + R^i_b r^b_{C/B}$$

$$\Downarrow$$

$$\begin{bmatrix} x^i_{C/O} \\ 0 \\ z^i_{C/O} \end{bmatrix} = \begin{bmatrix} x^i_{B/O} \\ 0 \\ z^i_{B/O} \end{bmatrix} + \begin{bmatrix} \cos(\theta) & 0 & \sin(\theta) \\ 0 & 1 & 0 \\ -\sin(\theta) & 0 & \cos(\theta) \end{bmatrix} \begin{bmatrix} x^b_{C/B} \\ 0 \\ z^b_{C/B} \end{bmatrix} \quad (1)$$

The horizontal spring force, in inertial coordinates, can be expressed:

$$X^i_s = \begin{cases} k_h(x^i_{M/O} - x^i_{C/O}) - c_h \dot{x}^i_{C/O} & \text{if } (*) \\ 0 & \text{otherwise.} \end{cases} \quad (2)$$

$(*)$: $x^i_{C/O} \geq x^i_{M/O}$. According to hypothesis (2), we have that $X^i_s < 0$ during craft-to-turbine contact. The vertical spring force in inertial coordinates is expressed

$$Z^i_s = k_v(z^i_{M/O} - z^i_{C/O}) + c_v(\dot{z}^i_{M/O} - \dot{z}^i_{C/O}). \quad (3)$$

2.2 The friction force

The friction force between the fictitious mass m_* and the turbine column is modelled as

$$Z_f^i = \begin{cases} Z_s^i & \text{if } (**) \\ \mu_k X_s^i \operatorname{sgn}(\dot{z}_{M/O}^i) & \text{otherwise.} \end{cases} \tag{4}$$

$(**)$: $|\dot{z}_{M/O}^i| < \epsilon$ and $|Z_s^i| \leq -\mu_s X_s^i$. The upper and lower row correspond to static and kinetic friction force, respectively. ϵ is chosen sufficiently small to avoid numerical problems in simulation, such as shattering. The parameter $sgn(\cdot)$ denotes the signum function. Recall that $X_s^i \leq 0$ so the friction force will always act against the motion and act as a stabilizer and damping of motion. Note that a discontinuity exist when toggling the regimes.

The equation of motion for the fictitious mass m_*, can be written

$$m_* \ddot{z}_{M/O}^i = Z_f^i - Z_s^i. \tag{5}$$

Note that due to equation (3), (4) and (5), the point M coincide with point C when turbine-contact is not present, hence $z_{M/O}^i = z_{C/O}^i$.

2.3 Decomposing the propulsion force

The propulsion forces are modelled in the inertial frame as

$$\begin{aligned} X_{prop}^i &= K_{BP} \cos(\theta), \\ Z_{prop}^i &= -K_{BP} \sin(\theta), \\ M_{prop}^i &= \frac{-L}{2} K_{BP} \sin(\theta), \end{aligned} \tag{6}$$

where $K_{BP} > 0$ denotes the propulsion bollard pull force. We assume that the propulsion force coincides with the water plane for $\theta = 0$. L denotes the air cushion length.

2.4 Air cushion pressure dynamics

The following notation and modelling of the air cushion is based on Sørensen and Egeland (1995). Let $P_u(t) + P_a$ denote the total air cushion pressure, where P_a and $P_u(t)$ denotes the atmospheric and the excess air cushion pressure, respectively.

For control purposes we define $\mu_u(t)$ as a uniform, non-dimensional dynamic cushion pressure variable:

$$\mu_u(t) = \frac{P_u(t) - P_0}{P_0}, \tag{7}$$

where P_0 denotes the equilibrium pressure.

$\Delta A_L(t)$ is our controller output and denotes the commanded dynamic leakage-area of the air cushion. The total leakage is expressed:

$$A_L(t) = A_{L,\,BIAS} + \Delta A_L(t), \tag{8}$$

where $A_{L,\,BIAS}$ is some mean operating value that allows two-sided control. In the absence of sea waves, the air cushion reaches its equilibrium point when $\Delta A_L(t) = 0$.

The dynamics for μ_u given in Sørensen and Egeland (1995) is written:

$$\begin{aligned} K_1\, \dot{\mu_u}(t) + K_3\, \mu_u(t) + \rho_{c0} A_c \dot{z}(t)_{B/O}^i - \rho_{c0} A_c x_{cp} \dot{\theta}(t) = \\ K_2\ \Delta A_L(t) + \rho_{c0}\, \dot{V}_0(t), \end{aligned} \tag{9}$$

with

$$\begin{aligned} K_1 &= \frac{\rho_{c0}\, h_0\, A_c}{\gamma \left(1 + \frac{P_a}{P_0}\right)},\ K_2 = \rho_{c0}\, c_n \sqrt{\frac{2P_0}{\rho_a}}, \\ K_3 &= \frac{\rho_{c0}}{2} \left(Q_0 - 2\, P_0\, q \frac{\partial Q_{in}}{\partial P}|_0 \right), \end{aligned} \tag{10}$$

where ρ_a, ρ_{c0} and A_c denotes ambient air density, equilibrium cushion density and air cushion area, x_{cp} denotes the longitudinal length between the inertial coordinate frame origin and the center of the air cushion pressure, Q_0 is the equilibrium air flow, $\frac{\partial Q_{in}}{\partial P}|_0$ is the linearised lift fan characteristic slope at the equilibrium point, which is always negative. q denotes the total number of lift fans that are running on the same, constant speed.

$\dot{V}_0$ is the wave volume pumping of the dynamic pressure. It is regarded a disturbance to the air cushion since it represents the sea wave volume inside the air cushion:

$$\dot{V}_0(t) = A_c\, \zeta_a\, \omega_0\, \frac{\sin \frac{k\,L}{2}}{\frac{k\,L}{2}}\, \cos(\omega_0 t), \tag{11}$$

where ζ_a and ω_0 denotes the wave height amplitude and sea wave frequency. $k = \frac{2\pi}{\lambda}$ denotes the wave number where λ is the sea wave length. As a side note, when modelling the vessel in transit we would use ω_e which is the wave frequency of encounter.

2.5 Motion in surge, pitch and heave:

The vessel motion in surge, pitch and heave consist of standard seakeeping equations of motion with radiation and wave excitation forces. The restoring forces are considered linear, following assumption 7.1 in (Fossen, 2011), for low-speed applications. The craft experience low speed during the docking phase. The same symbolic notation is also used.

The equations of motion are coupled with cushion pressure, spring forces and friction forces. A hydrostatic coupling between heave and pitch is neglected due to the chosen coordinate frame. The air cushion pressure is coupled with heave and pitch velocity. The work presented in this paper considers head seas which is reasonable since the orientation of the wind-turbine-ladder, which is where the bow docks the turbine, is placed accordingly. We consider the following control plant model, where the equation in surge can be expressed as

$$\begin{aligned} (m + A_{11})\, \ddot{x}_{B/O}^i(t) + B_{11}\, \dot{x}_{B/O}^i(t) = X_{prop}^i(t) + X_s^i(t) \\ + X_{waves}^i(t), \end{aligned} \tag{12}$$

and the motion in heave can be written as,

$$\begin{aligned} (m + A_{33})\, \ddot{z}_{B/O}^i(t) + B_{33}\, \dot{z}_{B/O}^i(t) + C_{33}\, z_{B/O}^i(t) \\ - A_c\, P_0\, \mu_u(t) = Z_{prop}^i(t) + Z_s^i(t) + Z_{waves}^i(t), \end{aligned} \tag{13}$$

while the pitch equation is given by

$$\begin{aligned} (I_{yy} + A_{55})\, \ddot{\theta}(t) + B_{55} \dot{\theta}(t) + C_{55} \theta(t) + x_{cp} A_c\, P_0\ \mu_u(t) \\ = M_{prop}^i(t) + z_{C/B}^b X_s^i(t) - x_{C/B}^b Z_s^i(t) + M_{waves}^i(t), \end{aligned} \tag{14}$$

where A_{ii}, B_{ii} and C_{ii} denotes the hydrodynamic added-mass-, water wave radiation- and hydrostatic coefficient in motion ii where $i = 1, 3, 5$ respectively denoting motion in surge, heave and pitch. Added mass and radiation terms

are frequency-dependent but are solved as coefficients using the Cumming equation (Faltinsen, 1990), (Fossen, 2011). m and I_{yy} denotes vessel mass and moment of inertia around the y-axis. X^i_{waves}, Z^i_{waves} and M^i_{waves} are the hydrodynamic wave excitation forces in surge, heave and pitch, respectively, and models for these can be found in Faltinsen (1990) and Fossen (2011).

3. CONTROL SYSTEM DESIGN

The control problem considered consist of minimizing the vertical craft motion by controlling the air cushion pressure. The pressure is not actuated directly but through varying the leakage area out of a set of vent valves as illustrated in equation (8) and (9).

3.1 State space model

The SISO system, expressed in equation (1) through (14) can be written on the following state space form:

$$\begin{aligned} \dot{\mathbf{x}}(t) &= \mathbf{A}\mathbf{x}(t) + \mathbf{B}u(t) + \mathbf{f}(\mathbf{x}(t)) + \mathbf{E}\mathbf{v}(t) \\ y(t) &= \mathbf{C}\mathbf{x}(t), \end{aligned} \tag{15}$$

where $\mathbf{A}\mathbf{x}(t)$ captures the unperturbed and uncontrolled dynamics of the craft when bow-to-turbine contact isn't present. Correspondingly $\mathbf{A}\mathbf{x}(t) + \mathbf{f}(\mathbf{x}(t))$ applies for the perturbed bow-turbine-contact case which includes wave excitation, water jet-propulsion, spring- and friction-forces. $\mathbf{B}u(t)$ and $\mathbf{E}\mathbf{v}(t)$ is the control force and disturbance force, respectively.

Momenta, cushion pressure and displacement will be used as states in a 9-dimensional state space vector $\mathbf{x} = [x_1\ x_2\ ...\ x_9]^T$, where
x_1 : Heave displacement, $z^i_{B/O}$
x_2 : Pitch angle, θ
x_3 : Heave momentum, $(m + A_{33})\dot{z}^i_{B/O}$
x_4 : Pitch angular momentum, $(I_{yy} + A_{55})\dot{\theta}$
x_5 : Dynamic cushion pressure, $\mu_u(t)$
x_6 : Surge displacement, $x^i_{B/O}$
x_7 : Displacement of mass m_*, $z^i_{M/O}$
x_8 : Surge momentum, $(m + A_{11})\dot{x}^i_{B/O}$
x_9 : Vertical momentum of mass m_*, $m_*\dot{z}^i_{M/O}$

The scalar control is defined as $u(t) := \Delta A_L(t)$. Note that a positive u correspond to a leakage area less than $A_{L,\,BIAS}$ (8) and vice versa. Heave velocity is our measurement, hence $y(t) = \mathbf{C}\,\mathbf{x}(t) = \frac{x_3(t)}{m+A_{33}}$. The initial state is $x(t_0) = [\mathbf{0}_{1x6}\ z^b_{C/O}\ \mathbf{0}_{1x2}]$, where $\mathbf{0}_{nxm}$ is the $n \times m$-dimensional zero matrix. The disturbance vector is expressed $\mathbf{v} = [Z^i_{waves}\ M^i_{waves}\ \dot{V}_0\ X^i_{waves}]^T$.

The system matrices $\mathbf{A}$, $\mathbf{B}$, $\mathbf{f}(\mathbf{x})$, $\mathbf{E}$ and $\mathbf{C}$ can be found in Appendix A.

3.2 Feedback control law

The following feedback controller is proposed:

$$u(t) = -ky(t) = -k\,\mathbf{C}\,\mathbf{x}(t), \tag{16}$$

where $k \in \mathbb{R}^+$ is the controller feedback gain.

4. RESULTS

We have designed a controller as specified in section 3. Physically, the controller input is a numerical integration of an accelerometers located at the centre-of-gravity (CG) acting in the z-direction. The output is the commanded vent valve leakage area $\Delta A_L(t)$. BCS results which exclusively deals with a free floating SES can be found in Auestad et al. (2014). All values on the $y-$axis are normalized.

4.1 Simulation results

Fig. 5 illustrates a test run that consist of three phases. The craft (point C) is initially located in front of the turbine (point M) and no contact exist. Also, since the fictitious mass m_* is implemented to capture the dynamics of the fender it was tuned using the trial and error approach to capture model-test-data response. m_* was set to 5 kg. The propulsion force, which initially is zero, is enabled at $t = 33$ s. At this time turbine contact is engaged. The BCS is active from $t = 66$s. The regular head sea wave has peak-to-peak wave height 2.4m and period 7.16s.

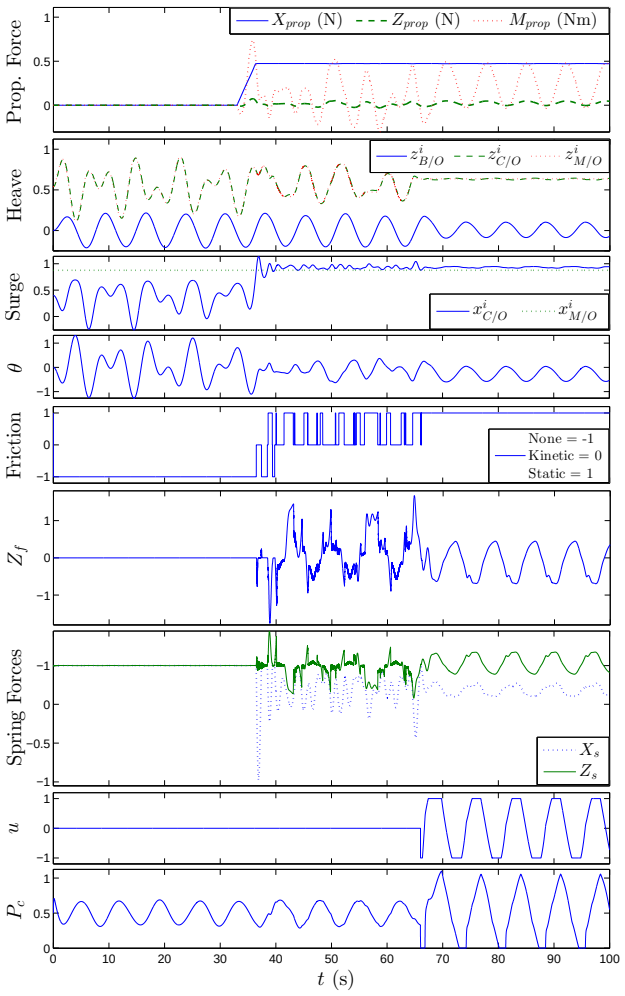

Fig. 5. Simulation run

The simulation can be summed up as follows:
Phase 1, $t \in (0, 33)$: The horizontal spring is uncompressed. In this sea state, the pitch (θ) resonance (3.3 s) is

triggered and results in fluctuations around the resonance- and the wave-frequency. The fictitious spring suspension follows the bow tip, hence $z^i_{M/O} = z^i_{C/O}$.

Phase 2, $t \in (33, 66)$: The propulsion force is thrusting the bow tip ($x^i_{C/O}$) towards the turbine, however, kinetic and static friction are fighting each other, leading the bow tip ($z^i_{C/O}$) to glide up and down the turbine. θ is damped due to friction.

Phase 3, $t \in (66, 100)$: The BCS is activated while maintaining the propulsion thrust force from phase 2. The amplitude of θ and $z^i_{B/O}$ indicates that motions in the entire vessel are significantly reduced. The friction force type are exclusively static and boarding of the turbine is safe since $z^i_{C/O}$ is fixed. The control system ensures that the system trajectories return to an equilibrium ($z^i_{C/O} \approx .0.6$).

4.2 Model-test craft

The performance of the control system has been investigated through model-testing (Fig. 2). This section is divided into two parts, one for regular seas and long-crested waves, and one for irregular seas described by a wave spectrum with distributed wave heights and periods.

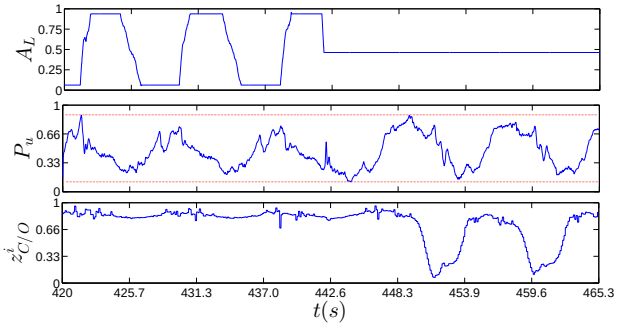

(a) $T_p = 8.5$s. BCS is turned *off* at $t = 441$s

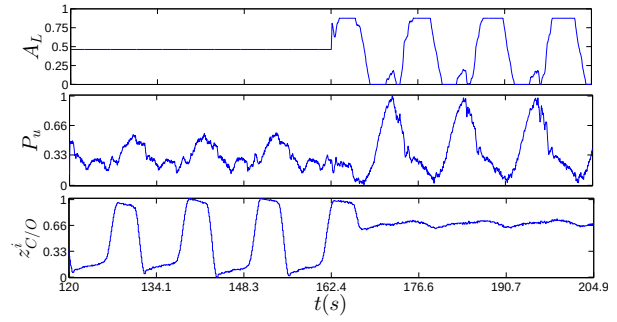

(b) $T_p = 11.7$s. BCS is turned *on* at $t = 162$s

Fig. 6. Time Series. $H_s = 3.2$m

Regular seas: Fig. 6 shows that the bow vessel tip is fixed to the turbine when the Boarding Control System is on while it is slipping up and down the turbine when the BCS is off (the system is uncontrolled). The peak-to-peak wave heights (H_s) are 3.2m. In Fig. 6a, the wave period (T_p) is 8.5s while it is 11.7s in Fig. 6b.

In Fig. 6a the amplitude of P_u decreases when the BCS is turned on, in contrast to Fig. 6b where the amplitude of P_u is increased when the BCS is turned on. This emphasize an important fact which differs from traditional RCS, since the BCS manipulates the pressure variations to be whatever is most beneficial to reduce vertical motions: for the shorter wave period case (Fig. 6b), the wave volume pumping (V_0) is dominating the disturbance in heave and consequently, the BCS manipulates the pressure variations by damping the disturbance pressure amplitude and by changing the phase to act in opposite direction of the heave velocity. For the case of the longer wave period Fig. 6b, the wave excitation force (Z^i_s) is the dominating disturbance and the BCS commands large pressure variations in counterphase of the heave velocity.

Irregular seas: The parameters H_s and T_p denote significant wave height and time period, respectively. In this case, the model-tank wave-generator produces a JONSWAP wave spectrum, Fossen (2011), parametrized with $H_s = 2.5$ m and $T_p = 7.5$ s.

Fig. 7 and 8 show the performance of the BCS in irregular seas by reducing vertical bow motions. This enables safe turbine access in higher sea states. Fig. 7 shows time series for a ten minute run, while Fig. 8 estimates of the Power Spectral Density (PSD) plot, obtained by the MATLAB function pwelch, for a 40 minute run. Decreased bow motion which results in increased safety during turbine boarding.

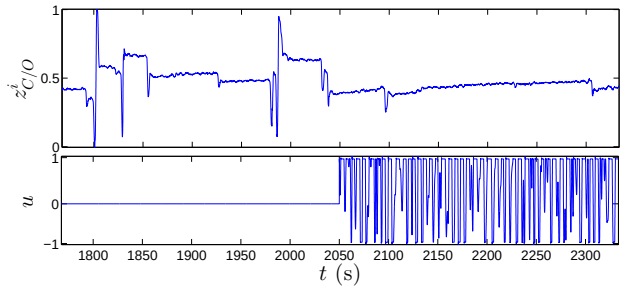

Fig. 7. Time series of the bow motion with and without the BCS active

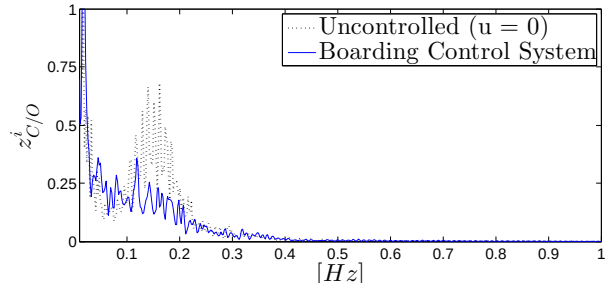

Fig. 8. PSD plot of the bow motion with and without the BCS active

5. CONCLUSIONS AND FURTHER WORK

The performance of the proposed BCS indicates that wind-turbine availability can be increased compared to the uncontrolled case. The model-test results in Fig. 6 indicate safe turbine access in up to 3.2 meter for regular waves, and up to 2.5 m significant for irregular waves (Fig. 7 and 8). Note that the bow experience some small slips during

the irregular sea case but turbine access is still regarded safe; in practice, all turbine transfer vessel experience some slips when pushing its sea wave limit OWA (2010) but it is the size of, and how frequently these appears, that are of interest. Unfortunately such limits are not yet classified but these crafts have a designated crew operator that signals the service personnel whether or not boarding is safe, and based on this, we regard the results given with the BCS active in Fig. 7, as safe. The Wave Craft prototype, Umoe Ventus is charted by Dong Energy on the wind-farm Borkum Riffgrund 1, in the Germany's north sea starting from March, 2015. Full-scale performance of the BCS will be published in the near future.

Appendix A. SYMBOLIC MATRICES

$$\mathbf{A} = \begin{bmatrix} \mathbf{A1}_{5x5} & \mathbf{0}_{5x4} \\ \mathbf{0}_{4x5} & \mathbf{0}_{4x4} \end{bmatrix}, \mathbf{f(x)} = \begin{bmatrix} \mathbf{0}_{2x1} \\ \mathbf{f1}_{3x1} \\ \mathbf{0}_{2x1} \\ \mathbf{f2}_{2x1} \end{bmatrix}, \mathbf{B} = \begin{bmatrix} \mathbf{B1}_{5x1} \\ \mathbf{0}_{4x1} \end{bmatrix},$$

$$\mathbf{E} = \begin{bmatrix} \mathbf{0}_{2x3} & \mathbf{0}_{2x1} \\ \mathbf{I}_{3x3} & \mathbf{0}_{3x1} \\ \mathbf{0}_{2x3} & \mathbf{0}_{2x1} \\ \mathbf{0}_{1x3} & 1 \\ \mathbf{0}_{1x3} & 0 \end{bmatrix}, \mathbf{C} = [\mathbf{C1}_{1x5} \quad \mathbf{0}_{1x4}], \tag{A.1}$$

where $\mathbf{I}_{nxm}$ denotes the nxm-dimensional identity matrix. Furthermore, using $\mathbf{A1} = \mathbf{A1}_{5x5}$:

$$\mathbf{A1} = \begin{bmatrix} 0 & 0 & \frac{1}{m+A_{33}} & 0 & 0 \\ 0 & 0 & 0 & \frac{1}{I_{yy}+A_{55}} & 0 \\ -C_{33} & 0 & \frac{-B_{33}}{m+A_{33}} & 0 & A_c P_0 \\ 0 & -C_{55} & 0 & \frac{-B_{55}}{I_{yy}+A_{55}} & -x_{cp} A_c P_0 \\ 0 & 0 & \frac{-\rho_{c0} A_c}{K_1(m+A_{33})} & \frac{x_{cp}\rho_{c0} A_c}{K_1(I_{yy}+A_{55})} & \frac{-K_3}{K_1} \end{bmatrix}$$

$$\mathbf{B1}_{5x1} = \begin{bmatrix} 0 & 0 & 0 & 0 & \frac{K_2}{K_1} \end{bmatrix}^T, \ \mathbf{C1}_{5x1} = \begin{bmatrix} 0 & 0 & \frac{1}{m+A_{33}} & 0 & 0 \end{bmatrix} \tag{A.2}$$

$$\mathbf{f1_{3x1}} = \begin{bmatrix} -K_{BP}\sin(x_2) + Z_s^i + Z_{waves}^i \\ -\frac{K_{BP} L \sin(x_2)}{2} + z_{C/B}^b X_s^i - x_{C/B}^b Z_s^i + M_{waves}^i \\ \rho_{c0} \dot{V}_0 \end{bmatrix},$$

$$\mathbf{f2_{2x1}} = \begin{bmatrix} K_{BP}\cos(x_2) + X_s^i + X_{waves}^i \\ Z_f^i - Z_s^i \end{bmatrix},$$

where

$$X_s^i = k_h \left(x_{M/O}^i - x_6 - \alpha \right) - c_h \left(\frac{x_8}{m + A_{11}} + \frac{\beta x_4}{I_{yy} + A_{55}} \right),$$

$$Z_s^i = k_v \left(x_7 - x_1 - \beta \right) + c_v \left(\frac{x_9}{m_*} - \frac{x_3}{m + A_{33}} + \frac{\alpha x_4}{I_{yy} + A_{55}} \right),$$

$$Z_f^i = \begin{cases} Z_s^i & \text{if } |\frac{x_9}{m_*}| < \epsilon \text{ and } |Z_s^i| \leq -\mu_s X_s^i \\ \mu_k X_s^i \operatorname{sgn}(\frac{x_9}{m_*}) & \text{else,} \end{cases}$$

and

$$\alpha = \alpha(x_2) = x_{C/B}^b \cos(x_2) + z_{C/B}^b \sin(x_2),$$
$$\beta = \beta(x_2) = -x_{C/B}^b \sin(x_2) + z_{C/B}^b \cos(x_2). \tag{A.3}$$

Appendix B. MAIN DIMENSIONS

Description	Full-scale	Model-scale
Length Over All	26.6 m	3 m
Width Over All	10.4 m	1.3 m
Draught (On-cushion)	2.77 (0.9) m	0.34 (0.1) m
Cargo Capacity	4 T	n.a.
Transit Speed	$\approx$ 40kn	n.a.

ACKNOWLEDGMENT

A special thanks to Umoe Mandal for sharing information and being helpful. Per S. Sodeland for helping out on modelling. The model-tests was sponsored by *Regionale forskningsfond Agder*, Norwegian Research Council and *Carbon Trust's OWA Competition*. All model-tests where conducted at the MC-Lab (AMOS, NTNU) and the Ship Model Tank, (SINTEF).

REFERENCES

Adams, J.D., Ernest, A.W., and Lewis, J. (1983). *Design, Development and Testing of a Ride Control System for the XR-ID Surface Effect Ship; Part I - Classical Control*. Maritime Dynamics, Inc., Tacoma, Washington, 98422.

Auestad, Ø.F., Gravdahl, J.T., Sørensen, A.J., and Espeland, T.H. (2014). Motion compensation system for a free floating surface effect ship. In *Proceedings of the 19th World Congress of the International Federation of Automatic Control, IFAC*. Cape Town, South Africa, August 24-29.

Butler, E.A. (1985). The surface effect ship. *Naval Engineers Journal*, 97(2), 200–258.

EEA (2008). Offshore wind energy: Action needed to deliver on the energy policy objectives for 2020 and beyond. *European and Environment and Agency*, Nov.

Faltinsen, O. (1990). *Sea Loads on Ships and Offshore Structures*. Cambridge University Press.

Fossen, T.I. (2011). *Handbook of Marine Craft Hydrodynamics and Motion Control*. John Wiley & Sons, Ltd, UK.

Kaplan, P. and Davies, S. (1978). System analysis techniques for designing ride control system for ses craft in waves. *5th Ship Contr. Syst. Symp. Annapolis, MD*.

Kaplan, P.B., Bentson, and Davis, S. (1981). *Dynamics and Hydrodynamics of Surface Effect Ships*. SNAMET Transaction Volume 89.

Lavis, D. (1998). Forty-plus years of hovercraft development. In *Proceedings of the 25th, Canadian Air Cushion Technology Society: CACTS '98*. Canadian Aeronautics and Space Institute.

OWA (2010). Offshore wind accelerator (owa) access competition overview and technical specification. *Carbon Trust*.

Sørensen, A.J. and Egeland, O. (1995). Design of ride control system for surface effect ships using dissipative control. *Automatica*, 31, 183 – 199.